

FORMATION OF KETENE (H₂CCO) IN INTERSTELLAR ANALOGOUS METHANE (CH₄)–CARBON MONOXIDE (CO) ICES: A COMBINED FTIR AND REFLECTRON TIME-OF-FLIGHT MASS SPECTROSCOPIC STUDY

SURAJIT MAITY^{1,2}, RALF I. KAISER^{1,2}, AND BRANT M. JONES^{1,2}

¹ W. M. Keck Research Laboratory in Astrochemistry, University of Hawaii at Manoa, Honolulu, Hawaii, HI 96822, USA

² Department of Chemistry, University of Hawaii at Manoa, Honolulu, Hawaii, HI 96822, USA

Received 2013 December 26; accepted 2014 March 25; published 2014 June 12

ABSTRACT

The formation of ketene (H₂CCO) in methane–carbon monoxide (CH₄–CO) ices was investigated upon its exposure to ionizing radiation in the form of energetic electrons at 5.5 K. The radiation-induced nonthermal equilibrium processing of these ices was monitored online and in situ via infrared spectroscopy complimented with post-irradiation temperature programmed desorption studies exploiting highly sensitive reflectron time-of-flight mass spectrometry (ReTOF) coupled with single photon fragment-free photo ionization (PI) at 10.49 eV. The detection of ketene in irradiated (isotopically labeled) methane–carbon monoxide ices was confirmed via the ν_2 infrared absorption band and substantiated during the warm-up phase based on sublimation profiles obtained from the ReTOF-PI spectra of the corresponding isotopic masses. The experiments conducted with the mixed isotopic ices of ¹²CD₄–¹³CO provide clear evidence of the formation of at least two ketene isotopomers (D₂¹²C¹³CO and D₂¹³C¹³CO), allowing for the derivation of two competing formation pathways. We have also proposed underlying reaction mechanisms to the formation of ketene based on kinetic fitting of the temporal evolution of the ketene isotopomers.

Key words: astrochemistry – cosmic rays – evolution – ISM: clouds – solid state: volatile

Online-only material: color figures

1. INTRODUCTION

The chemistry of the ketene molecule has been extensively investigated since the first discovery of diphenyl ketene in 1905 (Staudinger 1905) and the simplest member of this family, ethenone (commonly known as ketene; H₂CCO; Wilsmore 1907) as a highly reactive intermediate. For astronomers, ketene has also drawn considerable attention after its detection in the gas phase toward the star-forming region Sgr B2(OH) with abundances of 1.7×10^{14} molecules cm⁻² (Turner 1977; $f(\text{H}_2)$ of 2.0×10^{-10} considering H₂ $\sim 10^{24}$ molecules cm⁻²; Cernicharo et al. 1997). From here, ketene has proven to be an abundant interstellar molecule as it has been observed in a multitude of sources. Specifically, ketene has been monitored in the 1.3 mm band of the N and M positions of Sgr B2 by the Swedish-ESO Submillimetre Telescope molecular line survey yielding measured abundances $f(\text{H}_2)$ of 2.0×10^{-10} and 3.0×10^{-10} , respectively (Nummelin et al. 2000). Over the years, ketene has been observed in the Orion KL molecular cloud at levels of about 10^{14} molecules cm⁻² (Johansson et al. 1984) ($f(\text{H}_2) \sim 3 \times 10^{-7}$) and tentatively detected in TMC-1 (Matthews & Sears 1986) then later confirmed with measured abundances of 1.1×10^{13} molecules cm⁻² (Irvine et al. 1989) and 1.3×10^{13} molecules cm⁻² (Ohishi et al. 1991; $f(\text{H}_2) \sim 4 \times 10^{-11}$). Further, ketene was found in the gas phase of translucent clouds (CB 17, CB 24, and CB 228; Turner et al. 1999) with an estimated fractional abundance $f(\text{H}_2)$ of 1.1×10^{-9} following with observations in the prestellar core L1689B at abundances of about 10^{13} molecules cm⁻² (Bacmann et al. 2012) and extragalactic source PKS 1830–211 with similar fractional abundances of $f(\text{H}_2) = 10^{-10}$ to 10^{-9} (Muller et al. 2011). Recently, ketene was detected toward several deeply embedded protostars (AFGL 989, WL 22, NGC 6334I, NGC 7538 I1) with the observation that ketene is more abundant in the cooler extended

envelopes rather than the central hot core region based on the fractional abundances $f(\text{H}_2)$ of about 10^{-10} and the observed ratios of ortho-to-para spin states (Ruiterkamp et al. 2007). Consequently, the authors postulated the formation of ketene via grain-surface reaction and subsequent desorption to the gas phase. Here, three possible scenarios were proposed to explain the ketene abundances in the different regions of the interstellar medium. (1) Ketene in the hot core (Schoier et al. 2002; Turner 1991) could be the result of thermal desorption (sublimation) from grains. (2) Ketene with a constant distribution throughout the envelope (IRAS 16293–2422; Schoier et al. 2002) likely results from a combination of sublimation via thermal warming along with an additional desorption process (grain–grain collisions) in the outer region. (3) Ketene in the cooler outer envelopes (Cummins et al. 1986) could be evidence for ongoing processing of ices in the protostellar environment. Note that ketene has neither been identified in ices of young stellar objects (YSO) exploiting the Infrared Space Observatory (Gibb et al. 2004) nor in the ices of cloud cores and high-mass protostars in the *Spitzer c2d* ice survey (Boogert et al. 2008; Öberg et al. 2008, 2011; Pontoppidan et al. 2008). Here, the nondetection of ketene in interstellar ices is the result of overlapping with the most intense ketene absorption band (ν_2) with the fundamental of solid carbon monoxide at about 2137 cm⁻¹.

Further, ketene has been implicated as an important precursor in the formation of complex interstellar molecules such as acetic acid (CH₃COOH), acetamide (CH₃CONH₂), acetaldehyde (CH₃CHO), and methyl acetate (CH₃COOCH₃), as described by (Hudson & Loeffler 2013). Despite several reports on the astrochemical detection of ketene, experimental work on the formation of ketene in conditions simulating interstellar environments are sparse. The laboratory detection of ketene in astronomically relevant conditions was first reported by Haller & Pimentel, where ketene was detected as a product

during the photolysis of acetylene and dinitrogenmonoxide (N_2O) (1:1) in an argon matrix at 20 K via photolysis with 147 nm and 129.5 nm output of a xenon lamp (Haller & Pimentel 1962). Ketene was also detected as one of the broadband (220–1000 nm) photolysis products in mixtures of ozone and ethylene isolated within an argon matrix (Hawkins & Andrews 1983) and was found in the UV photolysis (<200 nm) experiment of ethylene oxide ($\text{C}_2\text{H}_4\text{O}$) in argon and nitrogen matrices (Schriver et al. 2004); interestingly, ketene was not observed when water was added to the ice mixtures. Recently, the formation of ketene was examined in various mixed ices consisting of analogous interstellar molecules such as acetylene (C_2H_2), ethylene (C_2H_4), methane (CH_4), carbon monoxide (CO), water (H_2O), carbon dioxide (CO_2), and oxygen (O_2 ; Hudson & Loeffler 2013). Here, the ice mixtures were exposed to ionization radiation in the form 0.8 MeV protons and $\text{Ly}\alpha$ photons (121.6 nm, $\sim 3 \times 10^{14}$ photons $\text{cm}^{-2} \text{s}^{-1}$). The radiation induced chemical processing with binary ices of hydrocarbons (C_2H_2 , C_2H_4 , CH_4) and oxygen containing (CO, H_2O , CO_2 , O_2) molecules were explored utilizing in situ infrared spectroscopy along with their isotopologues ices in order to separate ketene from the infrared absorption of carbon monoxide. As mentioned earlier, the strongest absorption band (ν_2) of ketene (H_2CCO , $A = 1.2 \times 10^{-16}$ cm molecule $^{-1}$; Hudson & Loeffler 2013) is positioned at 2136 cm^{-1} which overlaps with fundamental (ν_1) of carbon monoxide (CO, $A = 1.1 \times 10^{-17}$ cm molecule $^{-1}$; Garozzo et al. 2010) absorption feature at 2137 cm^{-1} . As such, the isotope labeling studies were conducted in order to detect ketene following exposure to ionizing radiation in binary ices of acetylene with oxygen, carbon dioxide, and water. Further, ketene was detected in the binary ices of methane (and ethylene) with oxygen containing molecules such as carbon monoxide, carbon dioxide, and oxygen upon exposure to both 0.8 MeV proton as well as $\text{Ly}\alpha$ photons. However, previous laboratory experiments in binary ice mixtures of methane–carbon monoxide ($\text{CH}_4\text{--CO}$) (Bennett et al. 2005a), carbon dioxide–ethylene ($\text{CO}_2\text{--C}_2\text{H}_4$; Bennett et al. 2005b), and methane–carbon dioxide ($\text{CH}_4\text{--CO}_2$; Bennett & Kaiser 2007a) exposed to ionizing radiation in the form of energetic electrons failed to detect ketene, as this molecule was most likely masked within the fundamental of carbon monoxide (from either the parent or product of the exposed ices) as these experiments were done using natural isotopes of C/H/O-bearing ices.

In the present study, we present compelling evidence of the formation of ketene in the interstellar analogue ices composed of methane and carbon monoxide ($\text{CH}_4\text{--CO}$). Here, selective isotopologues ices ($\text{CH}_4\text{--CO}$, $\text{CD}_4\text{--CO}$, $\text{CD}_4\text{--}^{13}\text{CO}$, $\text{CH}_4\text{--C}^{18}\text{O}$) were exposed to energetic electrons with an average dose of 1.2 eV per 16 amu, relevant to the lifetime of an interstellar icy grain within a cold molecular cloud prior to the warm up (star formation) phase. The online and in situ infrared spectroscopy confirms the detection of ketene based on the observed band positions and correlated frequency shifts within the irradiated isotopically labeled ices. Further, detection of ketene via infrared spectroscopy is confirmed via gas phase utilizing temperature program desorption studies coupled with single photon ionization ($E_{hv} = 10.49$ eV) reflectron time-of-flight mass spectrometry (ReTOF-PI). Evidence presented here suggests the formation of ketene in the bulk icy mantle of interstellar grains from the energetic processing via galactic cosmic rays followed by sublimation into the gas phase can rationalize the gas phase microwave spectroscopic observations of this molecule in various astrophysical environments mentioned above.

2. EXPERIMENT

The experiments were carried out in a contamination-free ultrahigh vacuum (UHV) chamber (Figure 1) evacuated to a base pressure of typically 2×10^{-11} Torr using magnetically suspended turbo molecular pumps backed by an oil free scroll pump (Bennett et al. 2013; Jones & Kaiser 2013; Kaiser et al. 2014). A polished silver mirror is then mounted to the cold finger and interfaced with indium foil to ensure thermal conductivity and subsequently cooling to a final temperature of 5.5 ± 0.1 K; the entire ensemble is freely rotatable within the horizontal center plane and translatable in the vertical axis via an UHV compatible bellow (McAllister, BLT106) and differential pumped rotational feed through (Thermoionics Vacuum Products, RNN-600/FA/MCO). Premixed gases of methane (CH_4 , Specialty Gases of America, 99.999%) and carbon monoxide (CO, Aldrich, 99.99%) with partial pressures of 100 Torr and 130 Torr, respectively, were then introduced into the main chamber through a glass capillary array held 30 mm in front of the silver mirror at a background pressure (uncorrected) of 5×10^{-8} Torr for approximately 3 minutes. The ice thickness was determined online and in situ via laser interferometry yielding 520 ± 20 nm utilizing an index of refraction of the mixed ice of 1.31 ± 0.02 at a helium–neon (HeNe) laser wavelength of 632.8 nm derived from numerical fitting of the observed intensity ratios (Westley et al. 1998). In order to derive the relative amount of each component for the binary mixture, the column densities were calculated utilizing a modified Lambert–Beer relationship (Bennett et al. 2004; Hudson & Moore 2001; Wada et al. 2006) with the absorption coefficients of 3.5×10^{-19} cm molecule $^{-1}$ and 1.1×10^{-17} cm molecule $^{-1}$ for the 4204 cm^{-1} ($\nu_1 + \nu_4$; CH_4) (Brunetto et al. 2008) and at 2090 cm^{-1} (ν_1 ; ^{13}CO) (Garozzo et al. 2010) bands. Here, the ratio ($\text{CH}_4\text{:CO}$) of the ice composition was determined as $3.5 \pm 0.5\text{:}2.5 \pm 0.5$. Isotopically mixed ices of $\text{CD}_4\text{--CO}$, $\text{CD}_4\text{--}^{13}\text{CO}$, and $\text{CH}_4\text{--C}^{18}\text{O}$ (CD_4 , CDN Isotopes, 99.9% D; ^{13}CO , Aldrich 99% ^{13}C ; C^{18}O , Aldrich 99% ^{18}O) were also exposed to ionizing radiation to confirm assignments via infrared frequency shifts and in the reflectron time-of-flight data via their shifts in mass-to-charge ratios.

The ices were then bombarded with 5 keV electrons at 5.5 ± 0.1 K for 1 hr at 30 nA over an area of 1.0 ± 0.1 cm^2 and an angle of incidence of 70° relative to the surface normal of the ice. The total dose deposited into the ice sample was determined from Monte Carlo simulations (CASINO; Drouin et al. 2007) taking into consideration the energy deposited from the back scattered electrons. The average dose deposited into the samples was determined as 1.2 ± 0.3 eV per 16 amu (4.9 ± 1.3 eV per CO molecule and $4.5 \text{ eV} \pm 1.4$ per CH_4 molecule). Here, the applied dose corresponds to approximately 10^5 yr in cold molecular clouds (Moore et al. 2001; Strazzulla et al. 1991). Note that the calculated penetration depth of the energetic electrons of 380 nm is less than the thickness of the sample of 520 ± 20 nm. Hence, the electrons only interact with the ice and not with the silver substrate. Furthermore, the density of the $\text{CH}_4\text{--CO}$ ice mixture was calculated as 0.81 g cm^{-3} based on the column-density-weighted fraction of their respective pure densities (0.47 g cm^{-3} CH_4 (Satorre et al. 2008), 1.029 g cm^{-3} CO (Bennett & Kaiser 2007b)) in the limit of volume additivity (Luna et al. 2012).

The irradiation-induced chemical processing of each binary ice mixture was monitored online and in situ via a Fourier Transform Infrared Spectrometer (Nicolet 6700) over a range of 6000 to 400 cm^{-1} at a resolution of 4 cm^{-1} . Each FTIR spectrum was

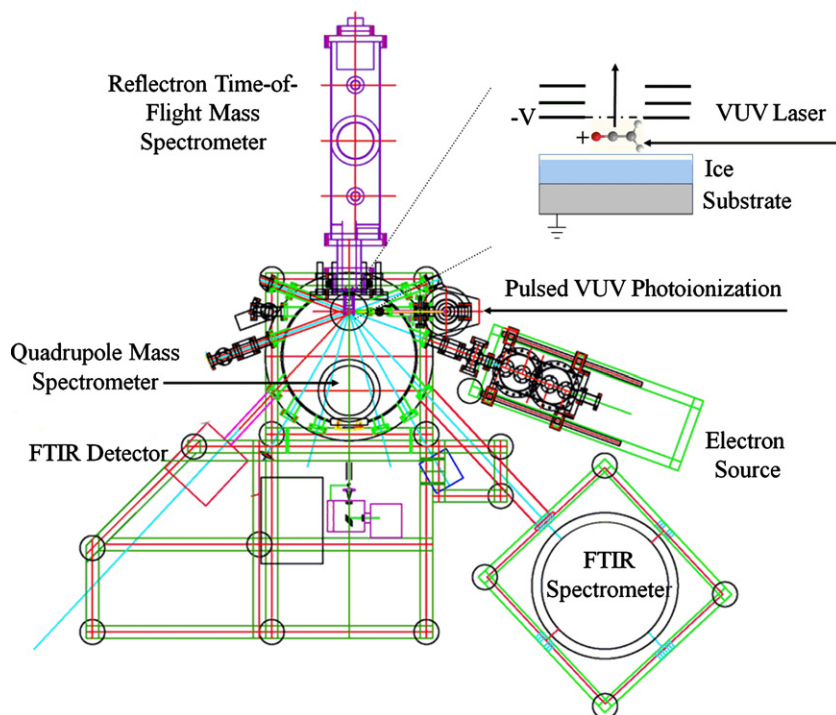


Figure 1. Top view schematic of the main chamber including analytical instruments, 5 keV electron source, and the cryogenic target (point of converging lines). The alignment of the target with the electron source and infrared spectrometer allow for simultaneous in situ measurements. After the irradiation, the cold head is rotated 180° to face the ReTOF mass spectrometer and warmed up, allowing the newly formed products to sublimate where upon they are ionized and mass analyzed. The inset (top right) shows the geometry of the ReTOF ion source lens with respect to the target and ionization laser.

(A color version of this figure is available in the online journal.)

recorded in the absorption–reflection–absorption mode (reflection angle = 45°) for 2 minutes resulting in a set of 30 infrared spectra during the radiation exposure. After irradiation, the sample was kept at 5.5 K for 1 hr; then, temperature programmed desorption (TPD) studies were conducted by heating the irradiated ices at a rate of 0.5 K min^{-1} to 300 K. Throughout the thermal sublimation process, the ice samples were monitored via infrared spectroscopy and reflectron time-of-flight mass spectroscopy separately, i.e., each experiment was conducted twice. Specifically, the molecules were monitored using a reflectron time-of-flight mass spectrometer (ReTOF) (Jordan TOF Products, Inc.) coupled with soft photoionization of the neutral molecules. Here, the products were ionized upon sublimation via single photon ionization exploiting pulsed (30 Hz) coherent vacuum ultraviolet (VUV) light at 118.2 nm (10.49 eV), the details of which have been described previously (Jones & Kaiser 2013; Kaiser, et al. 2014). The ions are detected utilizing a multichannel plate with a dual chevron configuration. From here the signals were amplified using a fast preamplifier (Ortec 9305) and shaped with a 100 MHz discriminator. The TOF spectra were recorded with a personal-computer-based multichannel scaler (FAST ComTec, P7888–1 E) using a bin width of 4 ns triggered at 30 Hz (Quantum Composers, 9518) with 3600 sweeps per mass spectrum correlated with a 1 K change in temperature. Additionally, subliming molecules were also probed via a quadrupole mass spectrometer (QMS) operating in a residual-gas analyzer mode (Extrel, Model 5221) in the mass range of 1–500 amu with electron impact ionization at 100 eV at a current of 1 mA and multiplier voltage of 2000 V. It should be mentioned here that both QMS and ReTOF measurements were conducted for the gas phase detection of the sublimed molecules during the temperature programmed des-

orption (TPD) studies. A comparison of the sublimation profiles derived using both techniques were also discussed.

3. RESULTS

3.1. Infrared Spectroscopy

Figure 2 depicts the infrared spectra of the binary ice consisting of methane (CH_4) and carbon monoxide (CO) along with the isotopologues ices ($\text{CD}_4\text{-CO}$, $\text{CD}_4\text{-}^{13}\text{CO}$, $\text{CH}_4\text{-C}^{18}\text{O}$) recorded before and after irradiation with the assignments, which are listed in Table 1 as well. The assignments of the newly formed molecules are confirmed based on the observed isotopic shifts of the peak positions in irradiated binary ices of $\text{CD}_4\text{-CO}$, $\text{CD}_4\text{-}^{13}\text{CO}$, and $\text{CH}_4\text{-C}^{18}\text{O}$. Figure 3(a) depicts the infrared spectra in the region of 2200 cm^{-1} to 2000 cm^{-1} , where isotopomers of ketene (H_2CCO) are observed via the ν_2 fundamental (CO stretching; Hudson & Loeffler 2013). In the case of irradiated $\text{CH}_4\text{-CO}$ ice, no ketene could be identified at 5.5 K attributed to the previously addressed overlapping of the ketene absorption band (ν_2) with the carbon monoxide fundamental absorption feature at 2137 cm^{-1} . However, as carbon monoxide sublimates at about 40 K, ketene can be detected via infrared spectroscopy upon warming to a suitable temperature. Specifically, Figure 3(b) shows the infrared spectra of the irradiated methane-carbon monoxide ices at 50 K after methane and carbon monoxide have completely sublimed. In the case of $\text{CH}_4\text{-CO}$ ice, ketene was confirmed via the observed absorption band at 2131 cm^{-1} (Table 2) in agreement with the value reported at 2136 cm^{-1} (Hudson & Loeffler 2013). In addition, ν_2 band of ketene was observed previously at 2148 cm^{-1} and 2144 cm^{-1} in argon and nitrogen matrices, respectively, containing ethylene oxide (Schriver et al. 2004),

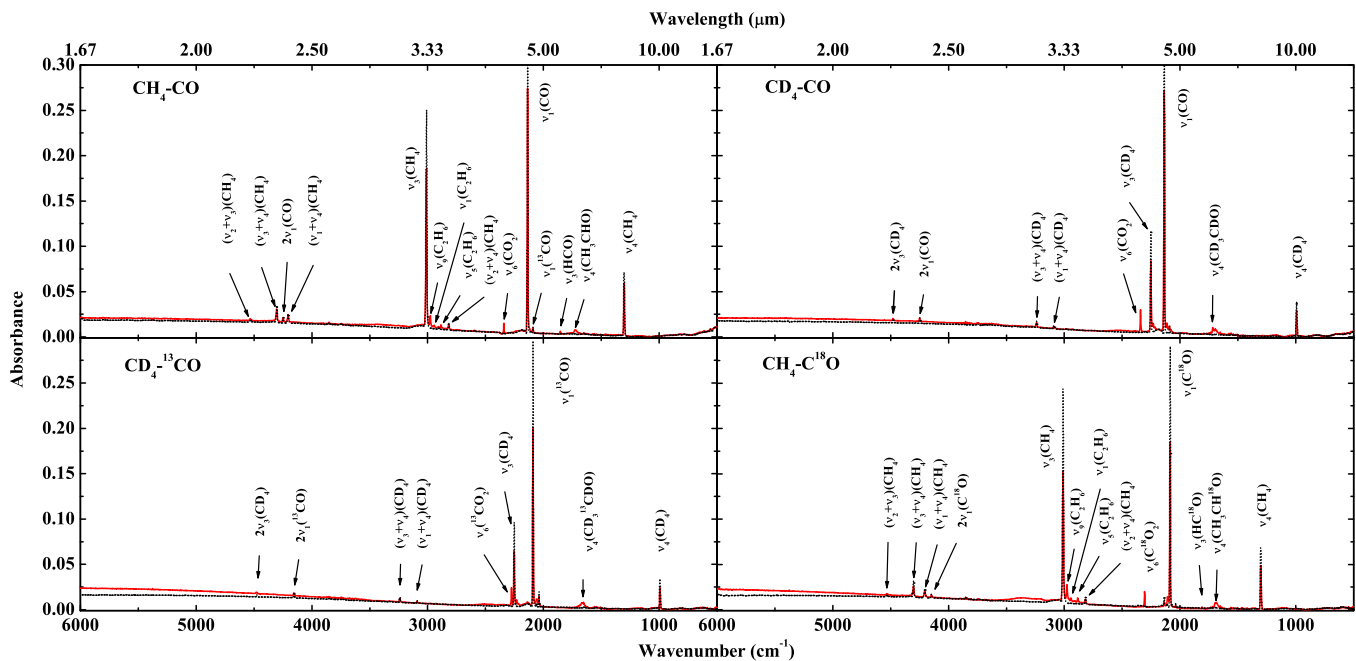


Figure 2. Infrared spectra of methane-carbon monoxide ices ($\text{CH}_4\text{-CO}$, $\text{CD}_4\text{-CO}$, $\text{CD}_4\text{-}^{13}\text{CO}$, and $\text{CH}_4\text{-C}^{18}\text{O}$) at 5.5 K before (black dotted line) and after (red solid line) the irradiation.

(A color version of this figure is available in the online journal.)

at 2150 cm^{-1} in an argon matrix containing ethylene and ozone (Hawkins & Andrews 1983), and at 2142 cm^{-1} in solid argon matrix (Haller & Pimentel 1962).

Additionally, ketene was also detected in the irradiated isotopically labeled ices due to the distinct frequencies of carbon monoxide and ketene. Previous studies identified isotopologues of ketene (D_2CCO , $\text{H}_2\text{}^{13}\text{C}^{13}\text{CO}$, $\text{H}_2\text{CC}^{18}\text{O}$) via absorptions (ν_2) at 2109 cm^{-1} , 2071 cm^{-1} , and 2107 cm^{-1} which are well separated from the absorption bands of corresponding carbon monoxide isotopologues (CO , ^{13}CO , C^{18}O), respectively, at 2136 cm^{-1} , 2091 cm^{-1} and 2088 cm^{-1} (Hudson & Loeffler 2013). In the present study; D_2CCO is observed at 2114 cm^{-1} in the radiation processed binary ice of $\text{CD}_4\text{-CO}$, and $\text{H}_2\text{CC}^{18}\text{O}$ is observed at 2104 cm^{-1} in the case of irradiated $\text{CH}_4\text{-C}^{18}\text{O}$ ice (Figure 3(a), Table 2) in agreement with the reported values (Hudson & Loeffler 2013). In the case of irradiated $\text{CD}_4\text{-}^{13}\text{CO}$ ice, due to the presence of two isotopes of carbon atoms (^{12}C and ^{13}C), four isotopomers of ketene (D_2CCO , $\text{D}_2\text{C}^{13}\text{CO}$, $\text{D}_2\text{}^{13}\text{CCO}$, $\text{D}_2\text{}^{13}\text{C}^{13}\text{CO}$) are possible. A deconvolution of the $2200\text{--}2050\text{ cm}^{-1}$ region after the irradiation of $\text{CD}_4\text{-}^{13}\text{CO}$ ice revealed two bands centered at 2052 cm^{-1} and 2060 cm^{-1} . The band positioned at 2052 cm^{-1} is assigned to $\text{D}_2\text{}^{13}\text{C}^{13}\text{CO}$ based on the isotopic shift of 65 cm^{-1} with respect to D_2CCO at 2114 cm^{-1} ; a similar frequency shift was identified previously between $\text{H}_2\text{}^{13}\text{C}^{13}\text{CO}$ (2071 cm^{-1}) and H_2CCO (2136 cm^{-1}) (Hudson & Loeffler 2013). Second, the band at 2060 cm^{-1} is assigned to the $\text{D}_2\text{C}^{13}\text{CO}$ isotopomer. Note that an isotopic shift of 8 cm^{-1} in the case of $\text{D}_2\text{}^{13}\text{C}^{13}\text{CO}$ with respect to $\text{D}_2\text{C}^{13}\text{CO}$ is reasonable based on the infrared absorptions HCCO and H^{13}CCO observed at 2026 cm^{-1} and 2020 cm^{-1} with an associated shift of 6 cm^{-1} (Hudson & Loeffler 2013). In regards to D_2CCO and $\text{D}_2\text{}^{13}\text{CCO}$, no infrared absorptions could be identified $\sim 2114\text{ cm}^{-1}$, implying that the formation of D_2CCO and $\text{D}_2\text{}^{13}\text{CCO}$ is negligible. Furthermore, we are unable to identify any other vibrational modes of ketene in the irradiated

isotopologues ices of methane-carbon monoxide attributing to their weak absorption coefficients (Hudson & Loeffler 2013).

3.2. ReTOF Mass Spectroscopy

In order to substantiate the infrared spectroscopic detection of ketene, we utilized temperature program desorption studies combined with highly sensitive reflectron time-of-flight mass spectroscopy coupled to fragment-free soft photoionization at 10.49 eV (ReTOFMS-PI). The sublimation profile of the ion signal at $m/z = 42$ amu in the irradiated $\text{CH}_4\text{-CO}$ ice recorded using ReTOF mass spectroscopy is shown in Figure 4(a). In addition, the ion trace at $m/z = 42$ amu during the warm up phase utilizing quadrupole mass spectroscopy with electron impact ionization (QMS-EI) is overlaid. The QMS traces at $m/z = 42$ amu reveal additional peaks at higher temperatures ($\sim 120\text{ K}$ and $\sim 150\text{ K}$), which are assigned to the electron-impact-induced fragmentation of $\text{C}_2\text{H}_4\text{O}$ isomers based on the correlation with the ReTOF ion signal at $m/z = 44$ amu (also overlaid in Figure 4(a)). The peaks at 120 K and 150 K in the QMS trace correlate to the observed ion signal at $m/z = 44$ via ReTOFMS-PI spectroscopy, confirming that the fragmentation of $\text{C}_2\text{H}_4\text{O}$ contributes to the QMS trace at $m/z = 42$ amu ($\text{C}_2\text{H}_2\text{O}$). The peak at 117 K at $m/z = 44$ amu has been assigned to the acetaldehyde (CH_3CHO ; IE = 10.23 eV) and vinyl alcohol (CH_2CHOH ; IE = 9.3 eV) at 147 K , as identified previously (Kaiser et al. 2014).

Additionally, signal at the corresponding mass of ketene isotopologues in the irradiated ices may also have a contribution from the ionization of C3 hydrocarbons. For example, in the irradiated $\text{CH}_4\text{-CO}$ system, ketene is expected at $m/z = 42$ amu, which overlaps with C_3H_6 isomers: propene (CH_3CHCH_2 ; IE = 9.7 eV) and cyclopropane (C_3H_6 ; IE = 9.9 eV). Similarly, in the irradiated $\text{CD}_4\text{-CO}$ system, ketene is expected at $m/z = 44$ amu, overlapping with C_3D_4 isomers: propyne (CD_3CCD ,

Table 1Infrared Absorption Features Recorded Before and After the Irradiation of Methane–Carbon Monoxide Ices ($\text{CH}_4\text{-CO}$, $\text{CD}_4\text{-CO}$, $\text{CH}_4\text{-C}^{18}\text{O}$, $\text{CD}_4\text{-}^{13}\text{CO}$) at 5.5 K

$\text{CH}_4\text{:CO}$		$\text{CD}_4\text{:CO}$		$\text{CH}_4\text{:C}^{18}\text{O}$		$\text{CD}_4\text{:}^{13}\text{CO}$		Assignment	Carrier	Ref.
Before (cm^{-1})	After (cm^{-1})	Before (cm^{-1})	After (cm^{-1})	Before (cm^{-1})	After (cm^{-1})	Before (cm^{-1})	After (cm^{-1})			
–		4479		–		4479		$2\nu_3(\text{CD}_4)$	overtone	1
4534				4533				$\nu_2 + \nu_3(\text{CH}_4)$	combination	1
4302		3240		4303		3240		$\nu_3 + \nu_4(\text{CH}_4)$	combination	2
4248		4249		4148		4156		$2\nu_1(\text{CO})$	overtone	3
4204		3090		4205		3090		$\nu_1 + \nu_4(\text{CH}_4)$	combination	1
	3253		2445		3256		2445	$\nu_3(\text{C}_2\text{H}_2)$	CH str.	1, 2
	3151		2372		3151		–	$\nu_3(\text{CH}_3)$	CH str.	1, 4
	3093		–		3095		–	$\nu_9(\text{C}_2\text{H}_4)$	CH_2 asym. str.	2
3011		2252		3011		2252		$\nu_3(\text{CH}_4)$	deg. str.	1, 2
	2978		2231		2978		2231	$\nu_{10}(\text{C}_2\text{H}_6)$	CH_3 deg. str.	1, 2
	2962		2216		2961		2216	$\nu_1(\text{C}_2\text{H}_6)$	CH_3 sym. str.	1, 2
	2943		–		2942		–	$\nu_8 + \nu_{11}(\text{C}_2\text{H}_6)$	combination	1, 2
	2920		2096		2918		–	$\nu_8 + \nu_{11}(\text{C}_2\text{H}_6)$	combination	1, 2
2905		2098		2905		–		$\nu_1(\text{CH}_4)$	sym. str.	1, 2
	2885		2080		2885		–	$\nu_5(\text{C}_2\text{H}_6)$	CH_3 sym str.	1, 2
2818		–		2818		2063		$\nu_2 + \nu_4(\text{CH}_4)$	combination	1, 2
	2748		1947		2742		1918	$\nu_2 + \nu_6(\text{C}_2\text{H}_6)$	combination	1, 2
2595		1978		2595		1979		$2\nu_4(\text{CH}_4)$	overtone	1, 2
	2341		2342		2339		2342	$\nu_6(\text{CO}_2)$	CO asym. str.	5
	2276		2277		–		2276	$\nu_6(^{13}\text{CO}_2)$	CO asym. str.	5
	–		–		2306		–	$\nu_6(\text{C}^{18}\text{O}_2)$	CO asym. str.	–
	–		–		2324		–	$\nu_6(^{18}\text{OC}^{16}\text{O})$	CO asym. str.	–
2137		2137		2137		2137		$\nu_1(\text{CO})$	CO str.	3, 5
	2090		2091		2087		2089	$\nu_1(^{13}\text{CO})$	CO str.	3
	1853		1796		1810		1774	$\nu_2(\text{HCO})$	CO str.	4
	1727		1717		1694		1669	$\nu_4(\text{CH}_3\text{CHO})$	CO str.	4
	1466		–		1465		–	$\nu_{11}(\text{C}_2\text{H}_6)$	CH_3 deform	1, 2
	1427		1024		1424		1022	$\nu_{12}(\text{CH}_3\text{CHO})$	CH_3 deform.	4
	1373		1052		–		1056	$\nu_6(\text{C}_2\text{H}_6)$	CH_3 sym deform.	1, 2
	1350		1158		1349		1158	$\nu_7(\text{CH}_3\text{CHO})$	CH_3 deform.	4
1302		993		1302		992		$\nu_4(\text{CH}_4)$	deg. str.	1, 2
	1120		1069		1120		1070	$\nu_8(\text{CH}_3\text{CHO})$	CH_3 deform.	4
	1091		–		1089		–	$\nu_2(\text{HCO})$	bending	4
	613		–		–		–	$\nu_2(\text{CH}_3)$	out of plane	1, 2

References. (1) Kaiser & Roessler (1997); (2) Bennett et al. (2006); (3) Jamieson et al. (2006); (4) Bennett et al. (2005a); (5) Bennett et al. (2004).

Table 2Peak Positions of Ketene Isotopomers Observed in the Processed Methane–Carbon Monoxide Isotopologues Ices ($\text{CH}_4\text{-CO}$, $\text{CD}_4\text{-CO}$, $\text{CD}_4\text{-}^{13}\text{CO}$ and $\text{CH}_4\text{-C}^{18}\text{O}$)

Ices	Molecules	Observed Position (cm^{-1})	Literature Position ^a (cm^{-1})	Assignments
$\text{CH}_4\text{-CO}$	H_2CCO	2131 ^b	2136	$\nu_2(\text{C}=\text{O}$ stretch)
	CO	2137	2136	$\nu_1(\text{C}=\text{O}$ stretch)
$\text{CD}_4\text{-CO}$	D_2CCO	2114	2109	$\nu_2(\text{C}=\text{O}$ stretch)
	CO	2137	2136	$\nu_1(\text{C}=\text{O}$ stretch)
$\text{CD}_4\text{-}^{13}\text{CO}$	$\text{D}_2\text{C}^{13}\text{CO}$	2060	...	$\nu_2(^{13}\text{C}=\text{O}$ stretch)
	$\text{D}_2^{13}\text{C}^{13}\text{CO}$	2052	...	$\nu_2(^{13}\text{C}=\text{O}$ stretch)
	^{13}CO	2089	2091	$\nu_1(^{13}\text{C}=\text{O}$ stretch)
$\text{CH}_4\text{-C}^{18}\text{O}$	$\text{H}_2\text{CC}^{18}\text{O}$	2104	2107	$\nu_2(\text{C}=\text{O}^{18}\text{O}$ stretch)
	C^{18}O	2087	2088	$\nu_1(\text{C}=\text{O}^{18}\text{O}$ stretch)

Notes. Observed band positions of isotopically labeled carbon monoxides are also listed for comparison.

^a Hudson & Loeffler (2013).

^b Observed band position after complete sublimation of CO during the warm-up phase.

IE = 10.36 eV), allene (CD_2CCD_2 , IE = 9.7 eV), and cyclopropene ($\text{CD}(\text{CD}_2)\text{CD}$, IE = 9.67 eV); see Table 3 for clarification. However, the irradiated $\text{CH}_4\text{-C}^{18}\text{O}$ allows for the separation of the C3 hydrocarbons as their respective mass-to-charge ratios are different from the corresponding ketene isotopomer ($\text{H}_2\text{C}_2^{18}\text{O}$). Ion signals corresponding to the isotopomers of

ketene are expected at $m/z = 44$ amu ($\text{C}_2\text{D}_2\text{O}$; $\text{CD}_4\text{-CO}$ system), at $m/z = 45$ amu ($^{13}\text{CCD}_2\text{O}$; $\text{CD}_4\text{-}^{13}\text{CO}$ system), and at $m/z = 44$ amu ($\text{C}_2\text{H}_2^{18}\text{O}$; $\text{CH}_4\text{-C}^{18}\text{O}$ system) based on the infrared spectroscopic data discussed above. Indeed, all mass-to-charge ratios are observed with identical sublimation profiles as shown in Figure 4(b); all exhibit a similar onset at 78 ± 1 K.

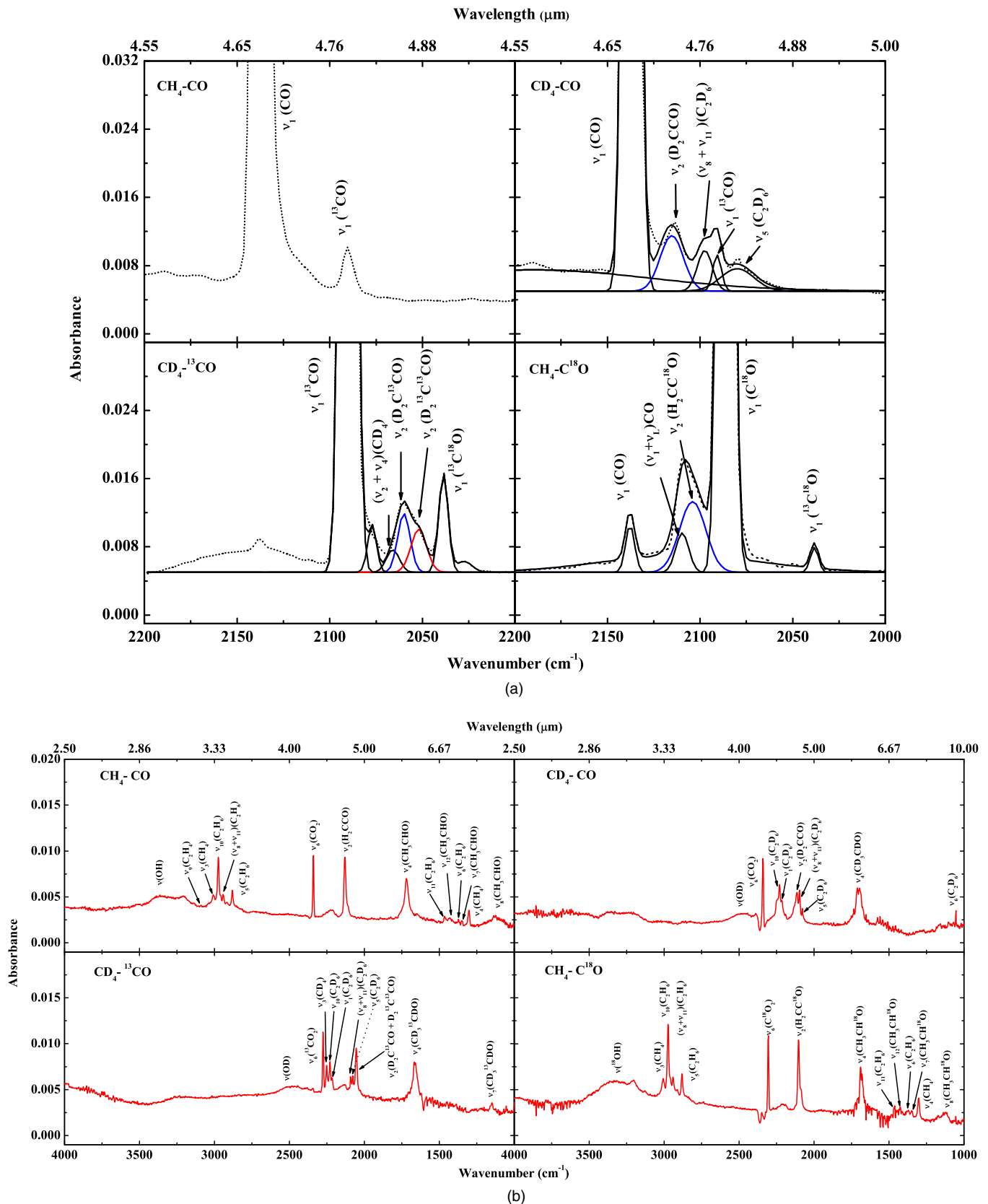


Figure 3. (a). Deconvolution of the 2200 cm^{-1} –2000 cm^{-1} region shown for $\text{CD}_4\text{-CO}$, $\text{CD}_4\text{-}^{13}\text{CO}$, and $\text{CH}_4\text{-C}^{18}\text{O}$ mixed ices elucidating the newly formed ketene (H_2CCO) isotopomers from adjacent absorption features. In the case of the $\text{CH}_4\text{-CO}$ system, ketene absorption band (ν_2) is hidden within the carbon monoxide fundamental at 2137 cm^{-1} . Infrared absorptions due to isotopomers of ketene are well separated from corresponding carbon monoxide absorption bands as assigned. (b) Infrared spectra of irradiated methane-carbon monoxide ices ($\text{CH}_4\text{-CO}$, $\text{CD}_4\text{-CO}$, $\text{CD}_4\text{-}^{13}\text{CO}$, and $\text{CH}_4\text{-C}^{18}\text{O}$) at 50 K after methane and carbon monoxide have completely sublimed.

(A color version of this figure is available in the online journal.)

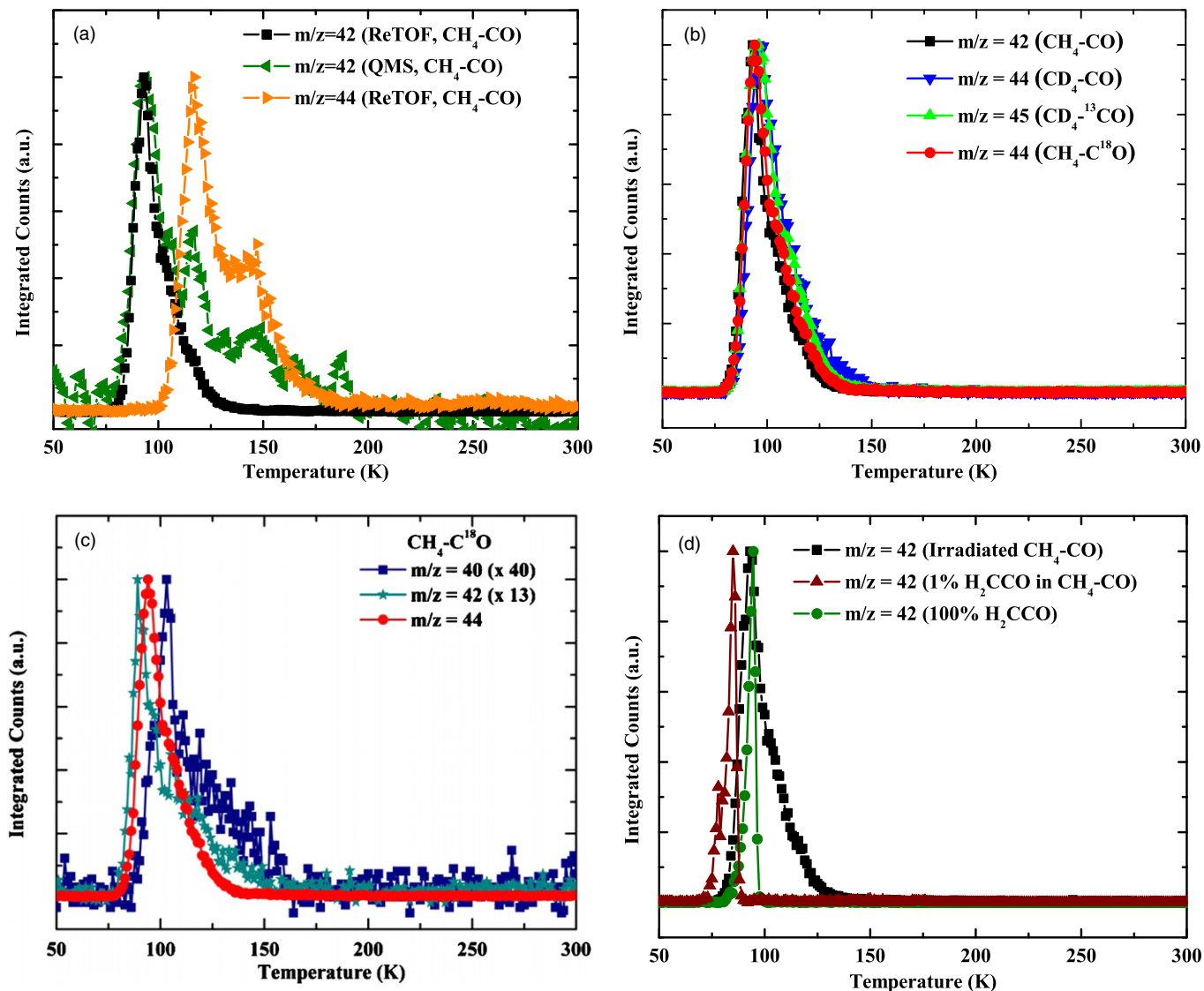


Figure 4. (a) Sublimation profile of integrated ion counts at $m/z = 42$ amu ($\text{C}_2\text{H}_2\text{O}$) recorded with ReTOFMS-PI and QMS-EI in the $\text{CH}_4\text{-CO}$ system. Also displayed is the sublimation profile of ion counts at $m/z = 44$ amu ($\text{C}_2\text{H}_4\text{O}$) from ReTOFMS-PI, which show the peaks at 120 K and 150 K are due to the fragmentation of $\text{C}_2\text{H}_4\text{O}$ parent. (b) Normalized sublimation profiles of integrated ion counts for the corresponding ketene isomers at $m/z = 42$ amu ($\text{C}_2\text{H}_2\text{O}$), 44 amu ($\text{C}_2\text{D}_2\text{O}$), 45 amu ($^{13}\text{CCD}_2\text{O}$), and 44 amu ($\text{C}_2\text{H}_2\text{C}^{18}\text{O}$) in irradiated ice systems of $\text{CH}_4\text{-CO}$, $\text{CD}_4\text{-CO}$, $\text{CD}_4\text{-}^{13}\text{CO}$, and $\text{CH}_4\text{-C}^{18}\text{O}$, respectively. (c) Sublimation profiles of ReTOF ion signal at $m/z = 40$ amu (C_3H_4), $m/z = 42$ amu (C_3H_6), and $m/z = 44$ amu ($\text{C}_2\text{H}_2\text{C}^{18}\text{O}$) in the irradiated $\text{CH}_4\text{-C}^{18}\text{O}$ ice. (d) Sublimation profile of integrated ion counts at $m/z = 42$ amu ($\text{C}_2\text{H}_2\text{O}$) subliming from the irradiated $\text{CH}_4\text{-CO}$ ice and for ketene (H_2CCO) calibration samples containing 1% ketene in $\text{CH}_4\text{-CO}$ (sample I) and for pure ketene (sample II).

(A color version of this figure is available in the online journal.)

Table 3

Mass-to-Charges (m/z) of $\text{C}_2\text{H}_2\text{O}$ Isotopomers in $\text{CH}_4\text{-CO}$, $\text{CD}_4\text{-CO}$, $\text{CD}_4\text{-}^{13}\text{CO}$, and $\text{CH}_4\text{-C}^{18}\text{O}$ Ices Are Compared to the Corresponding Isotopomers of C_3 Hydrocarbons (C_3H_4 , C_3H_6 , and C_3H_8)

Irradiated System	Products							
	Formula	m/z (amu)	Formula	m/z (amu)	Formula	m/z (amu)	Formula	m/z (amu)
$\text{CH}_4\text{-CO}$	$\text{C}_2\text{H}_2\text{O}$	42	C_3H_4	40	C_3H_6	42	C_3H_8	44
$\text{CD}_4\text{-CO}$	$\text{C}_2\text{D}_2\text{O}$	44	C_3D_4	44	C_3D_6	48	C_3D_8	52
$\text{CD}_4\text{-}^{13}\text{CO}$	$\text{C}_2\text{D}_2\text{O}$	44	C_3D_4	44	C_3D_6	48	C_3D_8	52
	$^{13}\text{CCD}_2\text{O}$	45						
	$^{13}\text{C}_2\text{D}_2\text{O}$	46						
$\text{CH}_4\text{-C}^{18}\text{O}$	$\text{C}_2\text{H}_2\text{C}^{18}\text{O}$	44	C_3H_4	40	C_3H_6	42	C_3H_8	44

In order to quantify the amount of C3 hydrocarbons that may contribute to the ion signal of ketene isotopomers (Table 3), a comparison of sublimation profiles of the ReTOF ion signals at $m/z = 40$ amu (C_3H_4 : allene, propyne, and cyclopropene), $m/z = 42$ amu (C_3H_6 : propene and cyclopropane), and $m/z = 44$ amu ($C_2H_2^{18}O$) in the irradiated $CH_4-C^{18}O$ system was made as this system allowed for the complete separation of hydrocarbon masses from C_2H_2O , the results of which are shown in Figure 4(c). Note that the ion signal at $m/z = 40$ amu was chosen to extrapolate the amount of equivalent C_3D_4 hydrocarbons that can be formed in the irradiated CD_4-CO and $CD_4-^{13}CO$ systems. Here, these mass-to-charges depicts total sublimation profiles with total integrated ion counts at $m/z = 40$ (C_3H_4), $m/z = 42$ (C_3H_6) are $3\% \pm 1\%$ and $9\% \pm 1\%$, respectively, compared to the total integrated ion counts at $m/z = 44$ ($C_2H_2^{18}O$). As such, only minor contributions of C_3H_6 isomers at $m/z = 42$ amu (C_2H_2O ; $m/z = 42$ amu) in the CH_4-CO system and C_3D_4 isomers at $m/z = 44$ amu (C_2D_2O ; $m/z = 44$ amu) in the CD_4-CO system are present. The contribution of propane (C_3H_8) and carbon dioxide (CO_2) at $m/z = 44$ amu in the above irradiated ices are excluded since their ionization energies (10.95 eV and 13.77 eV; Afeefy et al. 2010), respectively, are higher than the photon ionization energy of 10.49 eV.

In order to aid in the assignment of ketene (H_2CCO) to the ReTOF signal at $m/z = 42$ amu, we conducted TPD calibration experiments of methane-carbon monoxide ices containing 1% ketene (sample I) and of pure ketene (sample II), the results of which are shown in Figure 4(d). Ketene was prepared in the laboratory by pyrolysis of acetic anhydride at 510–550 K followed with purification and collection via successive cold traps (Fisher et al. 1953; Vogt et al. 1978). The peak ion signal corresponding to $m/z = 42$ amu (shown in Figure 4(d)) is observed at 85 K for sample I and at 95 K for sample II; note that the ion signal of $m/z = 42$ amu for the C_2H_2O isomer in the irradiated methane-carbon monoxide ice depict a maximum at 93 K, which lies between the maxima of the ion count profiles for sample I and sample II. Due to the similar sublimation temperatures, ketene contributes to the observed ion current in the irradiated ices. Note that compared to samples I and II in the irradiated sample, the subliming ketene depicts a tail extending up to about 130 K. This behavior is characteristic of higher molecular weight molecules synthesized during the irradiation process forming a “cap” and thus preventing ketene from subliming at its nominal temperature (Kaiser et al. 2010, 2014; Kim et al. 2010).

3.3. Correlation of Infrared and ReTOF data

In order to confirm the assignment of ketene (H_2CCO) in the collected ReTOF data described above, we examined the correlation of the infrared spectroscopic evidence with that of the sublimation profile for ions of C_2H_2O isotopologues during warm up as well. Recall that the formation of ketene was confirmed via the detection of ν_2 absorption features of H_2CCO at 2131 cm^{-1} (CH_4-CO ice at 50 K), along with D_2CCO at 2114 cm^{-1} (CD_4-CO ice), $D_2C^{13}CO$ at 2060 cm^{-1} ($CD_4-^{13}CO$ ice), and $H_2CC^{18}O$ ($CH_4-C^{18}O$ ice) at 2104 cm^{-1} (Table 2), immediately following irradiation at 5.5 K. Using the TPD ReTOF mass spectrometry, we also confirmed the detection of C_2H_2O ($m/z = 42$ amu), C_2D_2O ($m/z = 44$ amu), $D_2C^{13}CO$ ($m/z = 45$ amu), and $H_2C_2^{18}O$ ($m/z = 44$) in the methane-carbon monoxide isotopologue ices. Here, a direct comparison of the

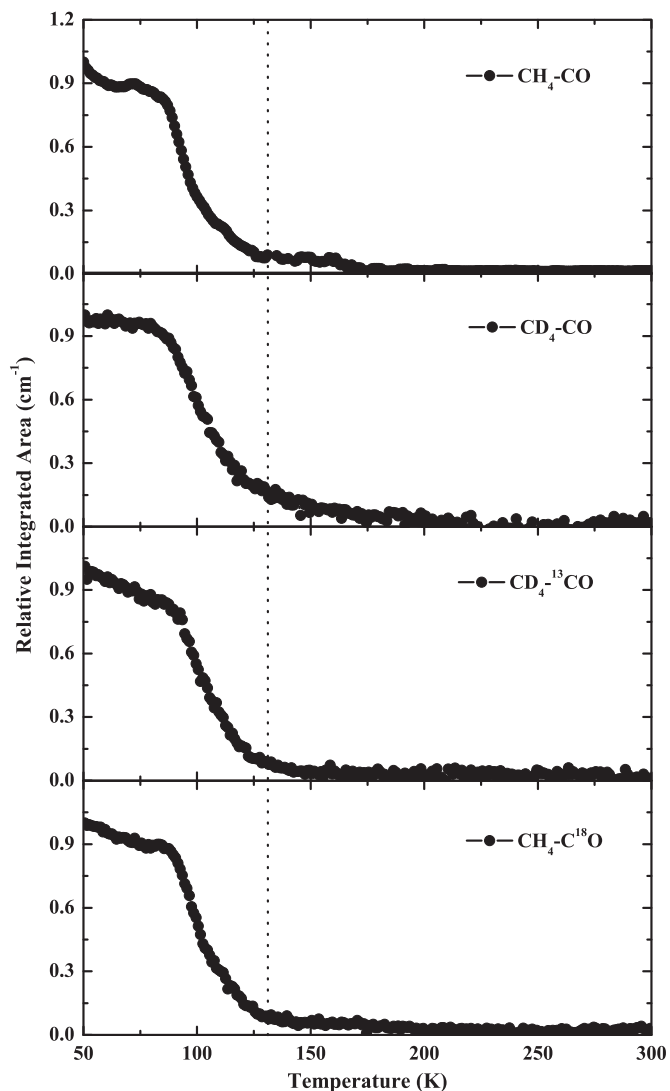


Figure 5. Temperature programmed desorption profiles derived from the integrated band area of ketene in the irradiated binary ices of CH_4-CO , CD_4-CO , $CD_4-^{13}CO$, and $CH_4-C^{18}O$. The dotted line at 130 K indicates the complete sublimation of ketene based on the TPD ReTOFMS-PI profiles.

sublimation profiles from infrared spectroscopic data (Figure 5) is made to those derived from ReTOF mass spectrometry and is shown in Figure 4(b). The integrated band area of the ketene ν_2 mode depicts a strong decline at 83 K (Figure 5), which correlates with the onset of the recorded ion profiles of $m/z = 42$ amu (Figure 4(b)). Note that the sublimation profiles of ketene isotopomers as shown in Figure 4(b) derived from ReTOF mass spectrometry depict the complete sublimation of ketene at ~ 130 K. The infrared absorption features show a strong decline until ~ 130 K, which correlate to the sublimation profiles of ketene isotopomers obtained from the ReTOF spectra. However, as shown in Figure 5, the infrared absorption at 2131 cm^{-1} in CH_4-CO ices is observable up to ~ 160 K (observed for all irradiated ices). The above observation suggests that infrared absorption at 2131 cm^{-1} beyond 130 K likely have contributions from high-mass ketenes. In the ReTOF spectra, we indeed observed ions with mass-to-charge ratios corresponding to C_3H_4O and C_4H_6O isotopomers with overlapping sublimation ranges and were assigned to unsaturated aldehydes and ketones (Kaiser et al. 2014), however, current results indicate that minor

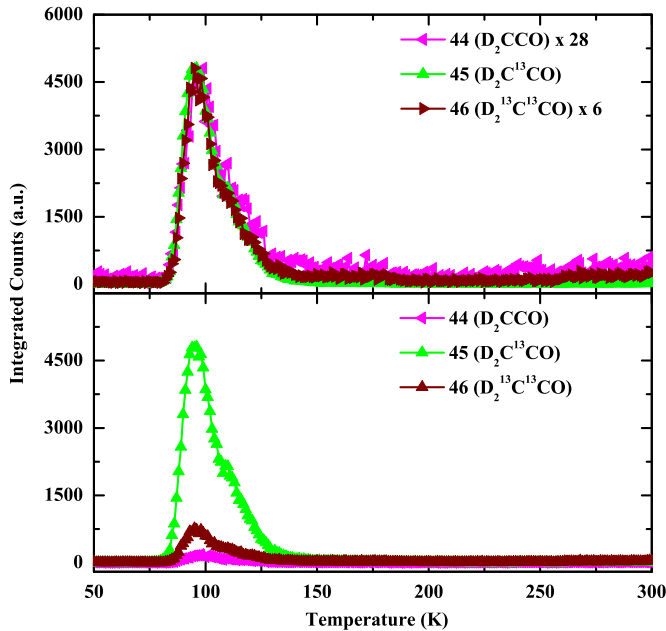


Figure 6. Sublimation profiles of the integrated ion counts of C_2H_2O isotopomers subliming from irradiated $CD_4-^{13}CO$ ice. Top: the sublimation profiles of C_2D_2O at $m/z = 44$ amu, $^{13}CCD_2O$ at $m/z = 45$ amu, and $^{13}C_2D_2O$ at $m/z = 46$ amu display identical sublimation profiles. Bottom: absolute integrated ion counts of C_2D_2O at $m/z = 44$ amu, $^{13}CCD_2O$ at $m/z = 45$ amu, and $^{13}C_2D_2O$ at $m/z = 46$ amu are shown.

(A color version of this figure is available in the online journal.)

contributions from higher mass ketenes (methyl ketene and dimethyl ketene) might also be present.

4. DISCUSSION

4.1. Reaction Pathways Based on ReTOF Data and IR Data

In the case of the $CD_4-^{13}CO$ system, mass-to-charge ratios at 44, 45, and 46 amu were observed and their respective sublimation profiles displayed in Figure 6. Here, due to the presence of two carbon atom isotopes (^{12}C and ^{13}C), three different masses corresponding to four possible isotopomers of ketene can be formed, i.e., D_2CCO (44 amu), $D_2C^{13}CO$ and $D_2^{13}CCO$ (45 amu), and $D_2^{13}C^{13}CO$ (46 amu). Consequently, the signal at $m/z = 45$ amu ($D_2C^{13}CO$) implies formation via one methane (CD_4) plus one carbon monoxide (^{13}CO) pathway. $D_2C^{13}CO$ was also identified at 2060 cm^{-1} using infrared spectroscopy. In conjunction, the observation of $D_2^{13}C^{13}CO$ (46 amu) implies synthesis stemming from two carbon monoxide (^{13}CO) molecules, which was also identified at 2052 cm^{-1} , as described earlier. Note, however, that the total integrated ion counts at $m/z = 44$ amu (D_2CCO) only accounted for $3\% \pm 1\%$ of the total ion signal from the most abundant product at $m/z = 45$ amu ($D_2C^{13}CO$). Here, C_3D_4 hydrocarbons can also contribute to the ReTOF ion signal at $m/z = 44$ amu, as described earlier. Also, recall that in the infrared spectra following irradiation, we were unable to detect any carbonyl absorption due to the D_2CCO molecule within the irradiated $CD_4-^{13}CO$ system. Consequently, the formation of ketene via a “two-methane molecule” pathway is not a major contributor. These observations conclude that ketene is formed in the irradiated methane–carbon monoxide ices via at least two different reaction pathways. (1) Following a “one methane plus one carbon monoxide” (formation of $D_2C^{13}CO$) pathway. (2) A

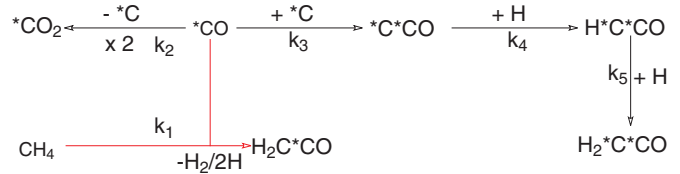


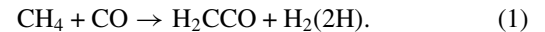
Figure 7. Kinetic scheme to fit the temporal evolution of ketene and carbon dioxide in irradiated methane–carbon monoxide isotopologues ices (CD_4-CO , $CD_4-^{13}CO$, and $CH_4-C^{18}O$). Here carbon atom originated from the carbon monoxide is marked as “*”. The reaction pathway highlighted in red represents “one methane and one carbon monoxide” mechanism and the remaining pathways (in black) correspond to “two carbon monoxide” mechanism.

(A color version of this figure is available in the online journal.)

reaction pathway involving a “two carbon monoxide” (formation of $D_2^{13}C^{13}CO$) route.

4.2. Kinetic Fits of Identified Reaction Pathways

Upon identifying two isotopomers of ketene in the irradiated $CD_4-^{13}CO$ ices, we can now formally elucidate the underlying mechanistic chemical routes. The formation routes are based on the experimental evidence identified from TPD ReTOF mass spectroscopy and from infrared spectroscopic results (Section 4.1), with the overall pathways identified in Figure 7. For this, the temporal profiles of the ketene isotopomers ($D_2C^{13}CO$ and $D_2^{13}C^{13}CO$) were traced along with carbon dioxide (Figure 8). A set of six coupled differential equations were utilized to numerically fit the temporal profiles by an iterative nonlinear optimization procedure adopted from Frenklach et al. (Frenklach et al. 1992) based on the identified reaction pathways shown above. Also note that the identical reaction schemes (Figure 7) are also utilized to fit the temporal profiles of ketene isotopomers observed in irradiated CD_4-CO and $CH_4-C^{18}O$ ices. The resulting rate constants are listed in Table 4. First, we would like to discuss the formation of $D_2C^{13}CO$ in the irradiated $CD_4-^{13}CO$ ice. Here we propose the formation of $D_2C^{13}CO$ following the incorporation of one methane and one carbon monoxide molecule with the subsequent elimination of molecular hydrogen and/or two hydrogen atoms.



This pathway follows pseudo-first order kinetics within a matrix cage and requires the intermediate formation of carbene (CH_2) (Kaiser & Roessler 1997). The derived rate constant (k_1) for reaction (1) was found to be $6.6 \pm 0.2 \times 10^{-6}\text{ cm s}^{-1}$ in the $CD_4-^{13}CO$ system. The required energy necessary for this endothermic reaction [$1.84\text{ eV molecule}^{-1}$ (H_2 elimination) and $6.36\text{ eV molecule}^{-1}$ ($2H$ elimination)] is well below the available energy of the impinging electron. As we have identified using infrared and ReTOF mass spectroscopy, the observation of $D_2^{13}C^{13}CO$ implies a “two carbon monoxide” pathway (Figure 7). Note that the temporal profile of $D_2^{13}C^{13}CO$ clearly shows a delayed growth, suggesting the involvement of multiple reaction steps. As previously suggested, carbon monoxide ($*CO$) can react via reaction (2), where energetically excited carbon monoxide molecules can react with neighboring carbon monoxide during irradiation (Jamieson et al. 2006); this is further supported in photolysis experiments of carbon monoxide ices (Gerakines & Moore 2001; Gerakines et al. 1996).



Here, we propose a similar reaction mechanism producing carbon dioxide and, more importantly, a source of carbon atoms.

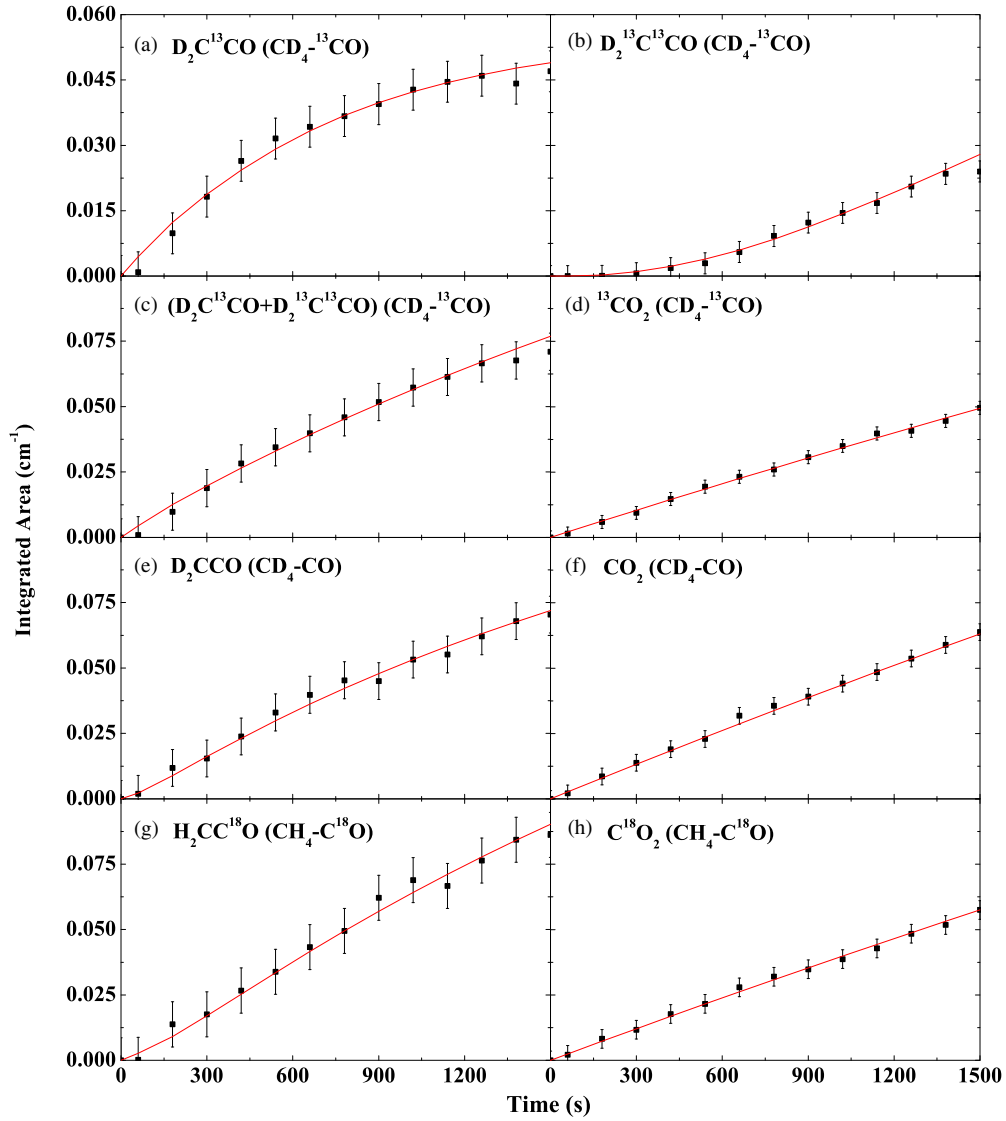


Figure 8. Fits of the temporal evolution of ketene isotopomers in $\text{CD}_4\text{-}^{13}\text{CO}$, $\text{CD}_4\text{-CO}$, and $\text{CH}_4\text{-C}^{18}\text{O}$ ices are shown during the electron irradiation at 5.5 K. The kinetic scheme as shown in Figure 7 is utilized to numerically fit the temporal profiles of (a) $\text{D}_2\text{C}^{13}\text{CO}$, (b) $\text{D}_2^{13}\text{C}^{13}\text{CO}$, and (d) $^{13}\text{CO}_2$ in $\text{CD}_4\text{-}^{13}\text{CO}$ system. In (c), the overall temporal profile of ketene in $\text{CD}_4\text{-}^{13}\text{CO}$ system is shown. The same scheme is used to fit the temporal profiles of ketene and carbon dioxide isotopologues in $\text{CD}_4\text{-CO}$ (E and F), $\text{CH}_4\text{-C}^{18}\text{O}$ (G and H) systems.

(A color version of this figure is available in the online journal.)

Table 4
Reaction Pathways and Derived Rate Constants Utilized to Fit the Temporal Evolutions of the Ketene and Carbon Dioxide Isotopomers in the Irradiated Methane–Carbon Monoxide Isotopologues Ices

Reactions	Rate Constants			
		$\text{CD}_4\text{-}^{13}\text{CO}$	$\text{CD}_4\text{-CO}$	$\text{CH}_4\text{-C}^{18}\text{O}$
$\text{CH}_4 + \text{*CO} \rightarrow \text{CH}_2\text{*CO} + 2\text{H}/\text{H}_2$	k_1	$(6.6 \pm 0.2) \times 10^{-6}$	$(2.0 \pm 0.2) \times 10^{-6}$	$(3.4 \pm 0.2) \times 10^{-6}$
$2\text{*CO} \rightarrow \text{*CO}_2 + \text{*C}$	k_2	$(2.2 \pm 0.1) \times 10^{-6}$	$(2.8 \pm 0.1) \times 10^{-6}$	$(2.6 \pm 0.1) \times 10^{-6}$
$\text{*C} + \text{*CO} \rightarrow \text{*C}_2\text{O}$	k_3	$(7.3 \pm 1.0) \times 10^{-4}$	$(2.0 \pm 1.0) \times 10^{-2}$	$(4.1 \pm 1.0) \times 10^{-2}$
$\text{*C}_2\text{O} + \text{H} \rightarrow \text{*CH*CO}$	k_4	$(3.9 \pm 0.4) \times 10^{-3}$	$(5.1 \pm 1.0) \times 10^{-2}$	$(2.4 \pm 1.0) \times 10^{-2}$
$\text{*CH*CO} + \text{H} \rightarrow \text{*CH}_2\text{*CO}$	k_5	$(1.5 \pm 0.5) \times 10^{-2}$	$(4.1 \pm 1.0) \times 10^{-2}$	$(1.2 \pm 1.0) \times 10^{-2}$
$\text{CH}_2\text{*CO} \rightarrow \text{X}$	k_6	$(1.3 \pm 0.5) \times 10^{-3}$	$(3.8 \pm 0.5) \times 10^{-4}$	$(2.7 \pm 0.5) \times 10^{-4}$

Notes. Here carbon atom originated from the carbon monoxide is marked as “*.” Units: k_1 , k_2 and k_3 are in cm s^{-1} (second order); k_4 , k_5 , k_6 are in s^{-1} (first order).

The temporal profile of carbon dioxide was included in the mechanistic scheme, as shown in Figure 8 with a derived rate constant (k_2) of $2.2 \pm 0.1 \times 10^{-6} \text{ cm s}^{-1}$ in $\text{CD}_4\text{-}^{13}\text{CO}$ system. The subsequent addition of the carbon atom produced

via reaction (2) to a carbon monoxide molecule can lead to the formation of the $^{13}\text{C}_2\text{O}$ radical via reaction (3).



We should mention here that the C_2O radical was not observed, implying very fast successive reactions with neighboring species. This radical was seen to be formed as a short lived intermediate during the electron irradiation of pure carbon monoxide ices (Jamieson et al. 2006) at 1988 cm^{-1} as well as observed via photolysis of carbon monoxide ice at 1990 cm^{-1} (Gerakines & Moore 2001). Reaction (3) is associated with a derived rate constant (k_3) of $7.3 \pm 1.0 \times 10^{-4}\text{ cm s}^{-1}$ in $CD_4\text{-}^{13}CO$ system.

From here, a barrier-less successive addition of atomic hydrogen, formed in reaction (1) or in the decomposition of methane as proposed previously (Baratta et al. 2003; Barberio et al. 2013; Bennett et al. 2006), with the ground state triplet C_2O diradical (reaction (4)) can ultimately lead to the formation of ketene H_2CCO (reaction (5)).



The rate constants for these reactions were derived as $3.9 \pm 0.4 \times 10^{-3}\text{ s}^{-1}$ (k_4) and $1.5 \pm 0.5 \times 10^{-2}\text{ s}^{-1}$ (k_5). Previous experiments were able to detect the HCCO radical at 2026 cm^{-1} in methane-carbon monoxide ices upon exposure to both 0.8 MeV proton and $Ly\alpha$ photons (Hudson & Loeffler 2013). However, the HCCO radical was not detected in the present experiments, possibly due to the lower irradiation dose (1.2 eV per 16 amu) compared to dose of 25 eV per 16 amu where the HCCO radical was observed. Additional reaction pathways considering the hydrogen atom addition to CO followed by the carbon atom addition leading to the formation of HCCO radical, as proposed previously (Charnley et al. 1997; Ruiterkamp et al. 2007), were also examined. However, these reaction pathways were found to be insignificant as no agreement with the experimental growth profiles of the ketene isotopomers could be made. In addition, the best fit of the temporal profile of ketene formed through reaction (1) i.e., via ‘‘one methane and one carbon monoxide’’ pathway is associated with a destruction pathway ($k_6 = 1.3 \pm 0.5 \times 10^{-3}\text{ s}^{-1}$) as well. This destruction pathway is reasonable since the hydrogenation of ketene by suprathermal hydrogen atoms can lead to the formation of other organic molecules such as acetaldehyde and ethanol (Bennett et al. 2005a; Ruiterkamp et al. 2007). The destruction of ketene can also be a result of dissociation due to energetic electrons.

As mentioned earlier, the same reaction scheme was used to fit the temporal profiles of ketene and carbon dioxide observed in irradiated $CD_4\text{-CO}$ and $CH_4\text{-C}^{18}O$ ices where only one isotope of carbon, hydrogen, and oxygen is present. Hence, reaction (1) and reactions (2)–(5) can result only one isotopomer of ketene (D_2CCO in $CD_4\text{-CO}$ ice and $H_2CC^{18}O$ in $CH_4\text{-C}^{18}O$ ice). The resulting rate constants of the optimized numerical fits in these systems are listed in Table 4. Here, the rate constants k_1 associated to reaction (1) in $CD_4\text{-CO}$ ($2.0 \pm 0.2 \times 10^{-6}\text{ cm s}^{-1}$) and $CH_4\text{-C}^{18}O$ ($3.4 \pm 0.2 \times 10^{-6}\text{ cm s}^{-1}$) systems are of the same order of magnitude as the $CD_4\text{-}^{13}CO$ ($6.6 \pm 0.2 \times 10^{-6}$) system. The rate constants of carbon monoxide dissociation via reaction (2) in the $CD_4\text{-CO}$ and $CH_4\text{-C}^{18}O$ systems are also consistent at $2.8 \pm 0.1 \times 10^{-6}$ and $2.6 \pm 0.1 \times 10^{-6}\text{ cm s}^{-1}$, respectively. The similar k_2 values in isotopologues ices validate the carbon monoxide decomposition pathway via the formation of carbon dioxide and the carbon atom. As listed in Table 4, the divergent rate constants k_3 and k_4 in these ices could possibly be due to the lack of a unique temporal profile for ketene formed via reactions (2)–(5). However, the rate of reaction (5) to the

formation of H_2CCO depict similar rate constants ($1.5 \pm 0.5 \times 10^{-2}$, $4.1 \pm 1.0 \times 10^{-2}$ and $1.2 \pm 1.0 \times 10^{-2}$ in $CD_4\text{-}^{13}CO$, $CD_4\text{-CO}$, and $CH_4\text{-C}^{18}O$, respectively).

5. CONCLUSIONS AND ASTROPHYSICAL IMPLICATIONS

Experiments relevant to the formation of ketene within simulated interstellar environments are sparse despite several reports on the detection of this molecule in extraterrestrial environments. Thus far, ketene has mostly been identified in photolysis experiments on: acetylene and N_2O (1:1) in an argon matrix (Haller & Pimentel 1962), ozone and ethylene isolated within an argon matrix (Hawkins & Andrews 1983), and ethylene oxide (C_2H_4O) in argon and nitrogen matrices (Schriver et al. 2004). Most recently, Hudson & Loeffler (2013) have reported the identification of ketene in bulk ice consisting of relevant interstellar molecules such as acetylene (C_2H_2), ethylene (C_2H_4), methane (CH_4), carbon monoxide (CO), water (H_2O), carbon dioxide (CO_2), and oxygen (O_2). The radiation (0.8 MeV protons and $Ly\alpha$ photons) induced chemical processing with binary ices of $C_2H_2\text{-}O_2$, $^{13}C_2H_2\text{-}O_2$, $C_2H_2\text{-}^{18}O_2$, $^{13}C_2H_2\text{-}H_2O$, $^{13}C_2H_2\text{-}CO_2$, $C_2H_4\text{-}O_2$, $C_2H_4\text{-}^{18}O_2$, $C_2H_4\text{-C}^{18}O_2$, $CH_4\text{-CO}$, $^{13}CH_4\text{-}^{13}CO_2$, and $CO\text{-}^{13}CH_4$ resulted the detection of ketene using infrared spectroscopy. The authors successfully identified ketene only in the isotopically labeled ices where the separation of the overlapping of the ν_2 fundamental of ketene with carbon monoxide (Hudson & Loeffler 2013) occurred. Several previous reports on similar binary ices exposed to ionization radiation were unsuccessful in identifying ketene due to the overlapping modes with carbon monoxide as these experiments were done using only natural isotopes (Bennett et al. 2005a, 2005b; Bennett & Kaiser 2007a).

Ketene has long been identified in the interstellar medium. However, the formation pathways of ketene in these environments have remained mainly speculative. A gas phase model (Millar et al. 1991) initially proposed the ion-molecular reaction of CH_3^+ with CO followed by proton elimination yields ketene. Unfortunately, this model was unable to reproduce the observed fractional abundances of ketene in the hotter regions of the Orion Compact Ridge. A gas phase model simulating ion-neutral reactions of ethylene ions ($C_2H_4^+$) with atomic oxygen followed by atomic hydrogen and proton elimination was later invoked and could successfully reproduce the fractional abundances of the Orion Compact Ridge (Millar et al. 1991); however, this model lacks experimental confirmation (Herbst & Leung 1989). Subsequent models suggested the protonation of ethylene ($C_2H_5^+$) followed by dissociative recombination with protonated ethane ($C_2H_7^+$) to produce the C_2H_3 (and C_2H_5) radical followed with a combination of atomic oxygen to produce ketene and atomic hydrogen in the gas phase (Charnley et al. 1992). Later experimental studies confirmed that this model does not reproduce ketene abundances (Hiraoka et al. 2000; Ruiterkamp et al. 2007). From here, grain-surface chemistry was suggested via hydrogenation of carbon monoxide followed by carbon atom reaction and then additional hydrogenation yielding ketene, i.e., $CO \rightarrow HCO \rightarrow HCCO \rightarrow H_2CCO$ (Charnley et al. 1997; Ruiterkamp et al. 2007). However, this reaction pathway has yet to be verified experimentally. The gas phase detection of ketene in the cold prestellar core of L1689B at temperatures $\sim 10\text{ K}$ suggests the formation of ketene with grain surface chemistry and subsequent nonthermal desorption via induced UV photons and cosmic ray impacts (Bacmann et al. 2012). As previously mentioned, ices containing a mixture of

hydrocarbons and oxygen-rich molecules exposed to ionization radiation in the form of 0.8 MeV protons and Ly α photons resulted in the detection of ketene within the bulk ices (Hudson & Loeffler 2013). The authors suggested that acetylene (HCCH) trapped in icy mantles containing oxygen bearing molecules such as O₂, H₂O, CO₂ can lead to the formation of ketene in the interstellar ices via reaction with atomic oxygen (radiolysis product of O₂, H₂O, CO₂). Furthermore, in ices containing ethylene (C₂H₄), the authors implied that ketene may be synthesized via the radiolysis ethylene to acetylene followed by reaction with atomic oxygen. However, reaction mechanisms relating to the formation of ketene in the ices containing methane and carbon monoxide were not discussed.

In the present experiments on methane–carbon monoxide ices exposed to ionizing radiation, two complementary detection techniques, *in situ* FTIR spectroscopy and single photoionization TPD ReTOF mass spectrometry were employed to analyze the endogenous synthesized products formed via radiation induced chemical processing. These coupled techniques confirmed the detection of ketene in irradiated ices of methane–carbon monoxide both in the solid state and gas phase following warm up. Here, in CH₄–CO ices, a maximum of $6.3 \pm 0.3 \times 10^{14}$ molecules (50 K) of ketene (derived with an *A* value of 1.2×10^{-16} molecule cm⁻¹ at 2131 cm⁻¹ (Hudson & Loeffler 2013)) were produced; this equates to $0.18 \pm 0.02\%$ and $0.26 \pm 0.03\%$ with respect to the initial amount of methane ($3.5 \pm 0.4 \times 10^{17}$ molecules cm⁻²) and carbon monoxide ($2.5 \pm 0.1 \times 10^{17}$ molecules cm⁻²) deposited.

Note that methane and carbon monoxide have long been identified within icy mantles in YSO observed exploiting the Infrared Space Observatory (ISO; Gibb et al. 2004) and in the ices of cloud cores and high-mass protostars in the *Spitzer c2d* ice survey (Boogert et al. 2008; Öberg et al. 2008, 2011; Pontoppidan et al. 2008). The interaction of ices with ionizing radiation simulating galactic cosmic rays (GCRs) the internal ultraviolet field within cold molecular clouds has repeatedly been demonstrated to chemically modify pristine ices (Bisschop et al. 2007; Garozzo et al. 2010; Geppert et al. 2006; Herbst & van Dishoeck 2009; Kaiser et al. 1997). The present experimental results show that ketene is an endogenous radiolytic byproduct of ices consisting of two simple, yet key, interstellar molecules, methane and carbon monoxide, thereby directly implicating the synthesis of ketene within interstellar ices. Within the plethora of interstellar ices observed thus far (Boogert et al. 2008; Gibb et al. 2004; Öberg et al. 2008, 2011; Pontoppidan et al. 2008), ketene has remained elusive as a direct consequence of the overlapping ketene absorption band (ν_2) with the carbon monoxide fundamental. Consequently, the reported solid phase abundances of carbon monoxide in interstellar ices may be an overestimation as the observed band at $4.67 \mu\text{m}$ ($\sim 2140 \text{ cm}^{-1}$) could have contribution from ketene as well. However, as shown here, the contribution is relatively minute as we have demonstrated that ketene accounted for only $0.18\% \pm 0.02\%$ of total deposited carbon monoxide in the present experiment with energetic doses relevant to the typical lifetime ($\sim 10^5$ – 10^6 yr) of an icy covered grain prior to the star forming (warm up phase) within a molecular cloud (Moore et al. 2001; Strazzulla & Johnson 1991). In the present experiment, we have identified two distinct ketene isotopomers (D₂C¹³CO and D₂¹³C¹³CO) in the irradiated mixed isotopic ices of CD₄–¹³CO using both infrared and ReTOF mass spectroscopy. The infrared spectroscopic data and subsequent kinetic fitting provide clear evidence of at least two different reaction pathways present

for the formation of ketene. Here, D₂C¹³CO is a product of one methane molecule (CD₄) and one carbon monoxide (¹³CO) molecule, (pathway (1), Figure 7). This novel formation route has never been considered for ketene synthesis in interstellar ices.

The authors thank the W. M. Keck Foundation, the University of Hawaii, and the NASA Exobiology Program MNX13AH62G. We also extend our thanks to Dr. Seol Kim for his assistance in the ketene synthesis.

REFERENCES

- Afeefy, H. Y., Liebman, J. F., & Stein, S. E. 2010, in *Neutral Thermochemical Data*, ed. P. J. Linstrom & W. G. Mallard (Gaithersburg, MD: National Institute of Standards and Technology)
- Bacmann, A., Taquet, V., Faure, A., Kahane, C., & Ceccarelli, C. 2012, *A&A*, **541**, L12
- Baratta, G. A., Domingo, M., Ferini, G., et al. 2003, *NIMPB*, **209**, 283
- Barberio, M., Vasta, R., Barone, P., Manico, G., & Xu, F. 2013, *WJCM*, **3**, 14
- Bennett, C. J., Brotton, S. J., Jones, B. M., et al. 2013, *AnaCh*, **85**, 5659
- Bennett, C. J., Jamieson, C., Mebel, A. M., & Kaiser, R. I. 2004, *PCCP*, **6**, 735
- Bennett, C. J., Jamieson, C. S., Osamura, Y., & Kaiser, R. I. 2005a, *ApJ*, **624**, 1097
- Bennett, C. J., Jamieson, C. S., Osamura, Y., & Kaiser, R. I. 2006, *ApJ*, **653**, 792
- Bennett, C. J., & Kaiser, R. I. 2007a, *ApJ*, **660**, 1289
- Bennett, C. J., & Kaiser, R. I. 2007b, *ApJ*, **661**, 899
- Bennett, C. J., Osamura, Y., Lebar, M. D., & Kaiser, R. I. 2005b, *ApJ*, **634**, 698
- Bisschop, S. E., Fuchs, G. W., van-Dishoeck, E. F., & Linnartz, H. 2007, *A&A*, **474**, 1061
- Boogert, A. C. A., Pontoppidan, K. M., Knez, C., et al. 2008, *ApJ*, **678**, 985
- Brunetto, R., Caniglia, G., Baratta, G. A., & Palumbo, M. E. 2008, *ApJ*, **686**, 1480
- Cernicharo, J., Lim, T., Cox, P., et al. 1997, *A&A*, **323**, L25
- Charnley, S. B., Tielens, A., & Millar, T. J. 1992, *ApJL*, **399**, L71
- Charnley, S. B., Tielens, A., & Rodgers, S. D. 1997, *ApJL*, **482**, L203
- Cummins, S. E., Linke, R. A., & Thaddeus, P. 1986, *ApJS*, **60**, 819
- Drouin, D., Couture, A. R., Joly, D., et al. 2007, *Scanning*, **29**, 92
- Fisher, G. J., MacLean, A. F., & Schnizer, A. W. 1953, *J. Org. Chem.*, **18**, 1055
- Frenklach, M., Wang, H., & Rabinowitz, M. J. 1992, *PrECS*, **18**, 47
- Garozzo, M., Fulvio, D., Kanuchova, Z., Palumbo, M. E., & Strazzulla, G. 2010, *A&A*, **509**, A67
- Geppert, W. D., Hamberg, M., Thomas, R. D., et al. 2006, *FaDi*, **133**, 177
- Gerakines, P. A., & Moore, M. H. 2001, *Icar*, **154**, 372
- Gerakines, P. A., Schutte, W. A., & Ehrenfreund, P. 1996, *A&A*, **312**, 289
- Gibb, E. L., Whittet, D. C. B., Boogert, A. C. A., & Tielens, A. G. G. M. 2004, *ApJS*, **151**, 35
- Haller, I., & Pimentel, G. C. 1962, *JChS*, **84**, 2855
- Hawkins, M., & Andrews, L. 1983, *JChS*, **105**, 2523
- Herbst, E., & Leung, C. M. 1989, *ApJS*, **69**, 271
- Herbst, E., & van Dishoeck, E. F. 2009, *ARA&A*, **47**, 427
- Hiraoka, K., Takayama, T., Euchii, A., Handa, H., & Sato, T. 2000, *ApJ*, **532**, 1029
- Hudson, R. L., & Loeffler, M. J. 2013, *ApJ*, **77**, 109
- Hudson, R. L., & Moore, M. H. 2001, *JGR*, **106**, 33275
- Irvine, W. M., Friberg, P., Kaifu, N., et al. 1989, *ApJ*, **342**, 871
- Jamieson, C. S., Mebel, A. M., & Kaiser, R. I. 2006, *ApJS*, **163**, 184
- Johansson, L. E. B., Andersson, C., Ellder, J., et al. 1984, *A&A*, **130**, 227
- Jones, B. M., & Kaiser, R. I. 2013, *J. Phys. Chem. Lett.*, **4**, 1965
- Kaiser, R. I., Eich, G., Gabrysch, A., & Roessler, K. 1997, *ApJ*, **484**, 487
- Kaiser, R. I., Maity, S., & Jones, B. M. 2014, *PCCP*, **16**, 3399
- Kaiser, R. I., Maksyutenko, P., Ennis, C., et al. 2010, *FaDi*, **147**, 429
- Kaiser, R. I., & Roessler, K. 1997, *ApJ*, **475**, 144
- Kim, Y. S., Bennett, C. J., Li-Hsieh, C., Brien, K. O., & Kaiser, R. I. 2010, *ApJ*, **711**, 744
- Luna, R., Satorre, M. Á., Domingo, M., Millán, C., & Santonja, C. 2012, *Icar*, **221**, 186
- Matthews, H. E., & Sears, T. J. 1986, *ApJ*, **300**, 766
- Millar, T. J., Herbst, E., & Charnley, S. B. 1991, *ApJ*, **369**, 147
- Moore, M. H., Hudson, R. L., & Gerakines, P. A. 2001, *AcSpe*, **57**, 843

- Muller, S., Beelen, A., Guélin, M., et al. 2011, *A&A*, **535**, A103
- Nummelin, A., Bergman, P., Hjalmarson, Å., et al. 2000, *ApJS*, **128**, 213
- Öberg, K. I., Boogert, A. C. A., Pontoppidan, K. M., et al. 2008, *ApJ*, **678**, 1032
- Öberg, K. I., Boogert, A. C. A., Pontoppidan, K. M., et al. 2011, *ApJ*, **740**, 109
- Ohishi, M., Kawaguchi, K., Kaifu, N., et al. 1991, in ASP Conf. Ser. 16, Atoms, Ions and Molecules: New Results in Spectral Line Astrophysics (San Francisco, CA: ASP), 387
- Pontoppidan, K. M., Boogert, A. C. A., Fraser, H. J., et al. 2008, *ApJ*, **678**, 1005
- Ruiterkamp, R., Charnley, S. B., Butner, H. M., et al. 2007, *Ap&SS*, **310**, 181
- Satorre, M. Á., Domingo, M., Millán, C., et al. 2008, *P&SS*, **56**, 1748
- Schoier, F. L., Jorgensen, J. K., Van Dishoeck, E. F., & Blake, G. A. 2002, *A&A*, **390**, 1001
- Schrivver, A., Coanga, J. M., Schrivver-Mazzuoli, L., & Ehrenfreund, P. 2004, *CP*, **303**, 13
- Staudinger, H. 1905, *Ber. Dtsch. Chem. Ges.*, **38**, 1735
- Strazzulla, G., & Johnson, R. E. 1991, in Comets in the Post-Halley Era, ed. R. L. Newburn, Jr., M. Neugebauer, & J. Rahe (The Netherlands: Springer), 243
- Strazzulla, G., Johnson, R. E., Newburn, R. L., Neugebauer, M., & Rahe, J. 1991, Comets in the Post-Halley Era, Vol. 167 (The Netherlands: Springer)
- Turner, B. E. 1977, *ApJL*, **213**, L75
- Turner, B. E. 1991, *ApJS*, **76**, 617
- Turner, B. E., Terzieva, R., & Eric, H. 1999, *ApJ*, **518**, 699
- Vogt, J., Williamson, A. D., & Beauchamp, J. L. 1978, *JChS*, **100**, 3478
- Wada, A., Mochizuki, N., & Hiraoka, K. 2006, *ApJ*, **644**, 300
- Westley, M. S., Baratta, G. A., & Baragiola, R. A. 1998, *JCP*, **108**, 3321
- Wilsmore, N. T. M. 1907, *FaTr*, **91**, 1938